Formation of stable ultra-thin pentagon Cu nanowires under high strain rate loading



2008 J. Phys.: Condens. Matter 20 335206

(http://iopscience.iop.org/0953-8984/20/33/335206)

J. Phys.: Condens. Matter **20** (2008) 335206 (6pp) doi:10.1088/0953-8984/20/33/335206

# Formation of stable ultra-thin pentagon Cu nanowires under high strain rate loading

**Vijay Kumar Sutrakar**[1] **and D Roy Mahapatra**[2,3]

[1] Mechanical Engineering Design Division, Aeronautical Development Establishment, Defence Research and Development Organization, New Thipasandara Post, Bangalore 560075, India
[2] Department of Aerospace Engineering, Indian Institute of Science, Bangalore 560012, India

E-mail: droymahapatra@aero.iisc.ernet.in

Received 21 April 2008, in final form 2 June 2008
Published 21 July 2008
Online at stacks.iop.org/JPhysCM/20/335206

**Abstract**

Molecular dynamics (MD) simulations of ⟨100⟩/{100} Cu nanowires at 10 K with varying cross-sectional areas ranging from $0.3615 \times 0.3615$ nm$^2$ to $2.169 \times 2.169$ nm$^2$ have been performed using the embedded atom method (EAM) to investigate their structural behaviors and properties at high strain rate. Our studies reported in this paper show the reorientation of ⟨100⟩/{100} square cross-sectional Cu nanowires into a series of stable ultra-thin pentagon Cu nanobridge structures with diameter of ∼1 nm under a high strain rate tensile loading. The strain rates used for the present studies range from $1 \times 10^9$ to $0.5 \times 10^7$ s$^{-1}$. The pentagonal multi-shell nanobridge structure is observed for cross-sectional dimensions <1.5 nm. From these results we anticipate the application of pentagonal Cu nanowires even with diameters of ∼1 nm in nano-electronic devices. A much larger plastic deformation is observed in the pentagonal multi-shell nanobridge structure as compared to structures that do not form such a nanobridge. It indicates that the pentagonal nanobridge is stable. The effect of strain rate on the mechanical properties of Cu nanowires is also analyzed and shows a decreasing yield stress and yield strain with decreasing strain rate for a given cross-section. Also, a decreasing yield stress and decreasing yield strain are observed for a given strain rate with increasing cross-sectional area. The elastic modulus is found to be ∼100 GPa and is independent of strain rate effect and independent of size effect for a given temperature.

(Some figures in this article are in colour only in the electronic version)

## 1. Introduction

The structural properties of metallic nanowires have been extensively investigated over the past decade. Understanding these properties is important in the context of nano-electronic device fabrications. The structures of ultra-thin nanowires of Au [1–6], Cu [7–9], Pb, Al [10–12], Ag [13], and Ti [14] have been investigated using MD simulations. These studies show that helical, multi-shelled, and filled structures exist in several face-centered-cubic (FCC) metals in the form of ultra-thin nanowires. Because of the strong surface effect, unique behaviors such as surface-stress-induced phase transformation [15] and lattice reorientation [16, 17] have also been observed. Nanowires are of great technological importance because of their unique structures, properties, and potential applications in nanoscale electronics, photonics, biological, and chemical sensors [18, 19]. In the recent years, various nano-devices have been developed from nanowires, such as nanolasers [20, 21], Field-effect transistors (FET) [22, 23], light emitting diodes [24] and quantized conductance atomic switches [25]. Nanowire sensors have also been fabricated for the highly sensitive and selective detection of biological and chemical species such as hydrogen [26], CO and $NO_2$ gases [27], proteins and DNA [28]. These nanowires components have even been integrated as address

[3] Author to whom any correspondence should be addressed.

 

decoders for nanosystems such as biological sensor arrays and nanocomputers [29].

Among all nanowires, metal nanowires have attracted a lot of interest because of their appealing properties such as high thermal and electrical conductivity, and quantized conductance [30–33]. In the previous work on Cu nanowires, atomistic simulations under various conditions have produced many different polygonal cross-section Cu nanowires [9], such as rectangular, pentagonal, and hexagonal ones. From electron diffraction, high resolution transmission electron microscopy (HRTEM), and power spectra (PS) results, Lisiecki *et al* [34] have shown that a decahedron model can explain the structure of the pentagonal Cu nanorods. Many studies on the structures of nanowires have shown that some nanoparticles are related to a decahedron model, e.g., in Ag [35], Ni [35], Au [35–38], and Cu [39, 40]. The coupled effects of geometry and surface orientation of Cu nanowires during mechanical loading at various strain rates and temperature have been analyzed in [41–48]. Mehrez and Ciraci [49] have reported the formation of hexagonal rings formed from {111} oriented Cu at 150 K. These hexagonal rings further transform into pentagonal rings during mechanical stretching. Sen *et al* [50] have performed an extensive first-principles study of nanowires with various pentagonal structures by using the pseudo-potential plane wave method within the framework of density functional theory. They have shown that nanowires of different types of elements, such as alkali, simple, transition and noble metals, and inert gas atoms have a stable structure made of a staggered pentagonal shape with a linear chain perpendicular to the planes of the pentagon and passing through their centers. This is due to the fact that the pentagonal quasi-1D nanowires have higher cohesive energy than many other 1D structural arrangements. Recently, Gonzalez *et al* [51] have shown, by their experimental and theoretical studies, that Cu nanowires formed by mechanical stretching exhibit structural relaxation forming pentagonal [110] Cu nanowires with a quantum conductance of $\sim 4.5G_0$. Also, García-Mochales *et al* [52, 53] have shown the formation of orientation and temperature-dependent pentagons of Ni nanowires using statistical MD studies of various initial orientations. However, the formation of a stable pentagonal multi-shell nanobridge structure under dynamic loading of [100]/{100} Cu nanowires has not been found previously. In addition, the size-dependent mechanical properties of such nanowires are not known in detail. Under a range of high strain rate loading, such pentagonal multi-shell nanobridge structures with enhanced mechanical properties have been found. This finding is reported in the present paper.

In the present paper, we show the reorientation of ⟨100⟩/{100} Cu nanowires into a stable pentagonal multi-shell nanobridge structure due to the application of high strain rate tensile loading. The effect of strain rate on Cu nanowires is also investigated to understand the variations in structural and mechanical properties, which show that the structures with a pentagonal multi-shell have a larger plastic deformation range and hence they are a stable structure. The structure is found to be stable over a range of cross-sectional dimensions. From the results we anticipate the application of pentagonal Cu nanowires even with diameter of ∼1 nm in nano-electronic devices.

## 2. Simulation method

The molecular dynamic simulation of copper nanowires using the embedded atom method (EAM) [54, 55] as the underlying model of inter atomic interaction is considered. In the EAM, the total energy $E$ for a system of atoms is written as

$$E = \sum_{i}^{N} F_i\left(\overline{\rho}_i\right) + \tfrac{1}{2}\sum_{j\neq i}^{N} \phi_{ij}\left(r_{ij}\right), \tag{1}$$

where the summations in equation (1) extend over the total number of atoms $N$ in the system, $F_i$ is the embedded function, $\overline{\rho}_i$ is the electron density at atom $i$, $\phi_{ij}$ is a pairwise interaction function and $r_{ij}$ is the distance between atom $i$ and $j$. In this work, the EAM potential developed by Mishin *et al* [56] is utilized, which accurately represents the elastic properties and surface energies of copper. More importantly, the potential accurately captures the stacking fault and twinning energies, which is critical in analyzing inelastic deformation.

Copper nanowires with square cross-section ⟨100⟩/{100} were created using the known lattice parameters of a bulk FCC crystal. The length of the wire was kept constant at 13 nm with six different cross-sectional dimensions of $0.3615 \times 0.3615$, $0.723 \times 0.723$, $1.0845 \times 1.0845$, $1.446 \times 1.446$, $1.8075 \times 1.8075$ and $2.169 \times 2.169$ nm$^2$ were considered for the simulation. The wires were first relaxed to equilibrium configurations using the conjugate gradient method; the wires were then thermally equilibrated at 10 K using the Nose–Hoover thermostat [57, 58] for 10 picosecond (ps) with a time step of 0.001 ps before being loaded under tension along the wire's axis and allowed to relax by holding the length of the wire unchanged. The nanowires are not relaxed to a zero stress state and the beginning of deformation are at a stress level of 1.5–8.0 GPa. A similar procedure was also used by Liang and Zhou [59] in the MD simulation during tensile deformation of Cu nanowires.

The higher initial residual stresses, which decrease with increasing cross-sectional dimensions of the nanowire because of the high surface-to-volume ratio and higher energy of the free-surfaces created by the fabrication/growth process, mean the wires are not at equilibrium. In order to obtain a stable structure during MD simulation the nanowires are allowed to relax. One end is fixed in the axial direction and the other end free of constraints, and temperature is kept constant during relaxation by rescaling the atomic velocities. Liang *et al* [43] found that ⟨100⟩/{100} Cu nanowires with cross-sectional dimensions $<2.17 \times 2.17$ nm$^2$ show ∼30% contraction in their length during relaxation and subsequently change from ⟨100⟩/{100} to ⟨110⟩/{111} orientations; these changes are observed up to cross-sectional dimensions of $<3.0 \times 3.0$ nm$^2$. In the present simulation, the length of the nanowires is kept constant by constraining both the ends, which restrict the transformation of nanowires from ⟨100⟩/{100} to the ⟨110⟩/{111} orientation during the relaxation process. As a result, one observes higher initial surface stresses in the nanowires. Stress decreases as the size of the nanowire increases and it finally vanishes as the nanowires become comparatively bulky. Metal nanowires with ⟨110⟩ axes and

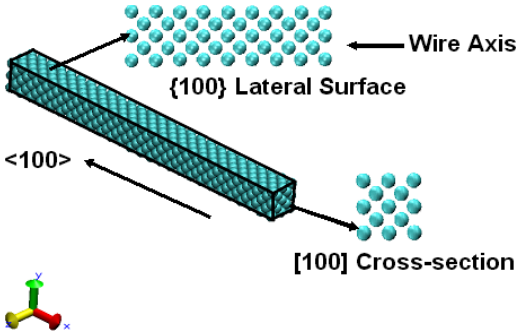


**Figure 1.** [100]/{100} Cu nanowire with $0.723 \times 0.723$ nm$^2$ cross-section.

{111} surfaces have been the most frequently observed in experiments (Rodriguez *et al* [60]; Liu and Bando [61]; Liu *et al* [62]; and Wang *et al* [63]) and atomistic simulations (Liang *et al* [43] and Diao *et al* [17]), whereas we have considered nanowires with a ⟨100⟩/{100} initial orientation in this paper. The ⟨110⟩/{111} configuration is more stable because it represents a lower energy state for FCC metal nanowires.

A uniaxial loading was performed by completely restraining one end of the wire, then by applying velocities to atoms along the loading direction that go linearly from zero at the fixed end to the maximum value at the free end, creating a ramp velocity profile. The initial velocities of particles are a Maxwell–Boltzmann distribution corresponding to a given temperature. It is given by

$$\frac{N(v)}{N} = \sqrt{\frac{m}{2\pi kT}} \exp\left(-\frac{mv^2}{2kT}\right), \tag{2}$$

where $N(v)$ denotes the number of particles which have velocity $v$, $k$ is Boltzmann's constant, and $T$ is temperature. To keep the system temperature the following correction is required;

$$v_i^{\text{new}} = v_i \sqrt{\frac{T_D}{T_A}}, \tag{3}$$

where $v_i^{\text{new}}$ is the velocity of the particle $i$ after correction (or velocity rescaling), $T_D$ and $T_A$ are the initial temperature and the evolved temperature of the system. This ramp velocity was used to avoid the emission of shock waves from the fixed end of the nanowire. The simulation procedure used in the present paper and as discussed above is taken from [48]. Park and Ji [48] have mentioned that the nanowire deformation mechanisms and mechanical properties are generally independent of the loading mechanism employed. Different strain rates ranging from $1 \times 10^9$ to $0.5 \times 10^7$ s$^{-1}$ were used for each nanowire. The equations of motion were integrated using the velocity Verlet algorithm [64]. All simulations were performed using an MD code called LAMMPS [65, 66] developed by Sandia National Laboratory. No periodic boundary conditions were used at any stage of the simulation, which was to capture accurately the relevant surface effects. The stresses were calculated using the virial theorem [67], which takes the form

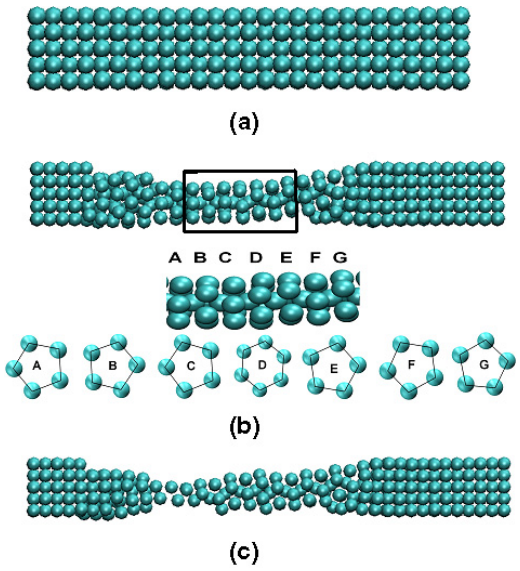


**Figure 2.** (a) Undeformed [100]/{100} Cu nanowires of cross-sectional dimensions $0.723 \times 0.723$ nm$^2$. (b) Formation of pentagon Cu nanowires of [100] cross-section after 2900 ps at a strain rate of $1.0 \times 10^9$ s$^{-1}$ and 10 K with a few hexahedral rings at the center cross-section. (c) Nanowire just before complete fracture showing a series of stable pentagon Cu lattice.

$$\sigma_{ij} = \frac{1}{V}\left(\frac{1}{2}\sum_{\alpha=1}^{N}\sum_{\beta\neq\alpha}^{N} U'\left(r^{\alpha\beta}\right)\frac{\Delta x_i^{\alpha\beta}\Delta x_j^{\alpha\beta}}{r^{\alpha\beta}} - \sum_{\alpha=1}^{N} m_\alpha \dot{x}_i^\alpha \dot{x}_j^\alpha\right), \tag{4}$$

where $N$ is the total number of atoms, $r^{\alpha\beta}$ is the distance between the two atoms $\alpha$ and $\beta$, $\Delta x_i^{\alpha\beta} = x_i^\alpha - x_i^\beta$, $U$ is the potential energy, and $V$ is the volume of the nanowire for the purpose of averaging. Engineering strain is used as a measure of deformation and defined as $(l - l_0)/l_0$, where $l$ is the instantaneous length of the wire and $l_0$ is the initial length of the wire obtained after the first step of energy minimization corresponding to the initial configuration. The yield stress and the yield strain are found at the point of initial yield, that is, when the first defect, which typically appears in the form of a partial dislocation, nucleates within the nanowires. The modulus of elasticity is calculated from the initial slope of the stress–strain curve for all the cases. The fracture strain is measured at the breaking point.

## 3. Results and discussions

In the present investigation, we have used square cross-sectional [100]/{100} Cu nanowires created out of a bulk FCC crystal. Figure 1 shows the cross-sectional and the lateral view of the structure prior to loading. Figure 2(a) shows the structure of the 0.723 nm cross-section nanowire before applying a strain rate loading of $1 \times 10^9$ s$^{-1}$. It can be seen that the nanowires loaded at this strain rate form necks and a nanobridge which has a pentagonal multi-shell structure; this is a new structure obtained under dynamic loading. The structure is illustrated in the snapshot at 2900 ps in figure 2(b). Portions of the nanobridge are marked with a rectangular box and shown in the close-up next to the deformed nanowire

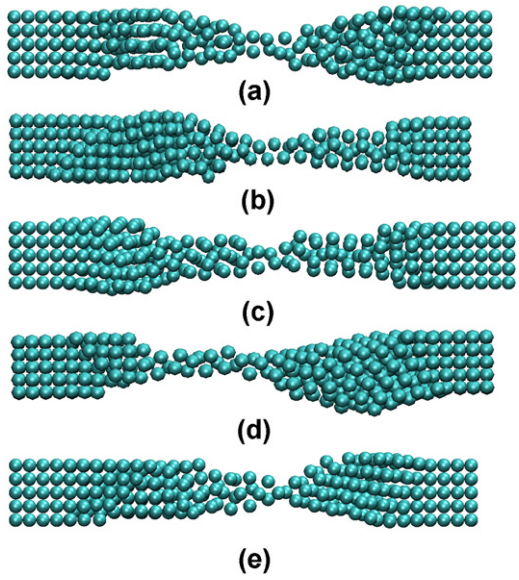


**Figure 3.** Deformed structure of [100]/{100} Cu nanowires of cross-sectional dimensions $0.723 \times 0.723$ nm$^2$ a temperature of 10 K and strain rates of (a) $0.5 \times 10^7$ s$^{-1}$, (b) $1.0 \times 10^7$ s$^{-1}$, (c) $0.5 \times 10^8$ s$^{-1}$, (d) $1.0 \times 10^8$ s$^{-1}$, and (e) $0.5 \times 10^9$ s$^{-1}$.

snapshots in figure 2(b). The nanobridges are marked as A, B, C, D, E, F, and G and the corresponding sectional view of each of the pentagonal shell structure is also shown in figure 2(b). However, because of the high strain rate, the square cross-sectional {100} nanowires reorient into a {100} pentagonal multi-shell structure; this is shown in the snapshot in figure 2(b). Further elongation in the nanowires shows the formation of a stable {100} pentagonal multi-shell structure over several atomic lattices, which is comprised of parallel {111} planes, as shown in figure 2(c). In the present finding, at larger strains under the applied high strain loading, the nanowire is unable to support the reoriented pentagonal multi-shell structure and an unstable chain with 1–3 atoms forms in which the atoms move in a helical, zigzag pattern. In other FCC structures, such an unstable chain with a few atoms is formed before complete fracture of the structure, in which atoms moves in a helical, zigzag pattern as observed by Sanchez-Portal *et al* [68] using first principle simulations and by Park and Zimmerman [46] using MD simulations. The onset of the helical, zigzag chain with 1–3 atoms indicates instability in the nanowires; fracture occurs soon after.

To examine the effect of the loading rate upon the stability of the nanobridge, we analyze the deformation process of the $0.723 \times 0.723$ nm$^2$ cross-section nanowire loaded at varying strain rates of $1.0 \times 10^9$, $0.5 \times 10^9$, $1 \times 10^8$, $0.5 \times 10^8$, $1.0 \times 10^7$, and $0.5 \times 10^7$ s$^{-1}$. As shown in figure 3, a loading rate of $0.5 \times 10^7$, $1 \times 10^8$, and $0.5 \times 10^9$ s$^{-1}$ produces reorientation of the structure from [100]/{100} to the atomic thick chain without any crystalline structure, indicating an instability in the nanowires whereupon further loading causes complete fracture of the structure without much plastic deformation. However, during the deformation of nanowires at a strain rate of $1 \times 10^7$ and $0.5 \times 10^8$ s$^{-1}$, the [100]/{100} Cu nanowire first reorients into a {100} pentagonal multi-shell nanobridge structure, and

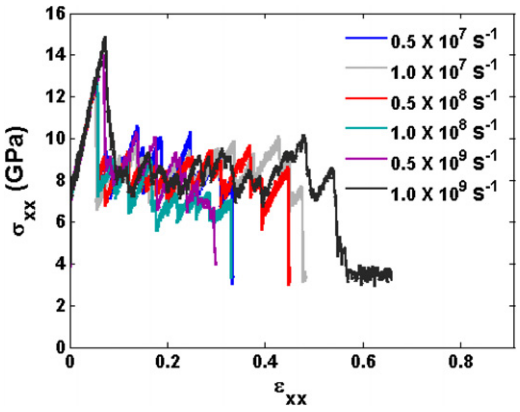


**Figure 4.** Stress–strain curve of [100]/{100} Cu nanowires of cross-sectional dimensions $0.723 \times 0.723$ nm$^2$ at various strain rates and 10 K.

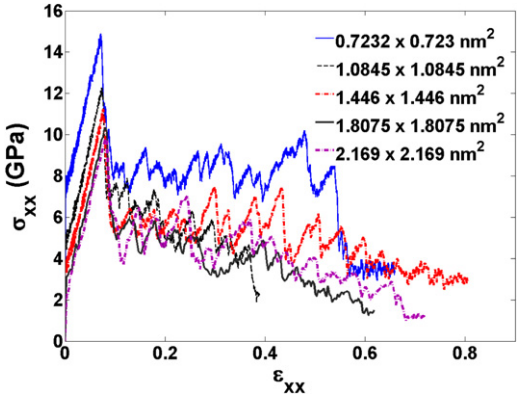


**Figure 5.** Stress–strain curve for strain rate of $1 \times 10^9$ s$^{-1}$ and 10 K for various cross-sectional dimensions of the Cu nanowires.

further loading caused the formation of stable {111} pentagonal multi-shell nanobridge structures with an unstable thick atom chain, which shows the instability of the nanowires before fracture. The absence of the pentagonal multi-shell structures at strain rates of $0.5 \times 10^7$, $1 \times 10^8$, and $0.5 \times 10^9$ s$^{-1}$ shows exceptions, which indicate that large surface stresses [15] and lateral surface orientation [48] play significant roles in the formation of stable nanobridges. Figure 4 also shows that the structure which forms pentagonal structure has a larger plastic strain and subsequently larger failure strain as compared to the structure which does not form such stable structures.

Stress–strain curves for all the nanowires with various strain rates are obtained and quantities such as yield stress, yield strain, elastic modulus and fracture strain due to formation of the pentagonal multi-shell nanobridge are compared. Since the elongation of the nanobridge is significant, it helps in explaining the stability of the nanowire with such a nanostructure. Figure 4 shows the larger plastic strain for all cases where the pentagonal multi-shell nanobridge structure formed in the $0.726 \times 0.726$ nm$^2$ Cu nanowire. The strain rate of $1 \times 10^9$ s$^{-1}$ produces the maximum yield stress. A decrease in the yield stress is observed with decreasing strain rate. A similar trend of decreasing yield strain is also observed with a decreasing strain rate for increasing cross-sectional dimensions of the nanowire as shown in figure 5.

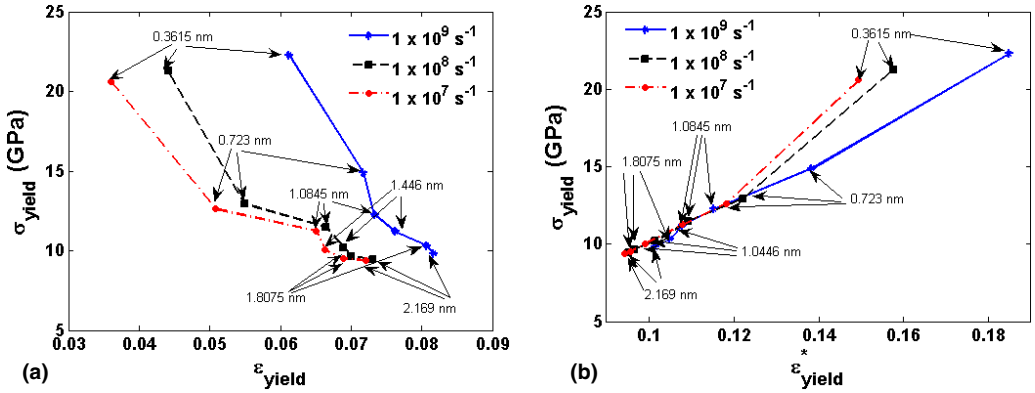


**Figure 6.** (a) Yield stress versus yield strain and (b) yield stress versus equilibrium yield strain (true yield strain) at various strain rates and cross-sectional dimensions of the Cu nanowires. The arrows indicate the initial cross-sectional dimensions.

A Cu nanowire structure with $0.726 \times 0.726$ nm$^2$ cross-sectional dimensions and the highest applied strain rate of $1 \times 10^9$ s$^{-1}$ shows a maximum fracture strain of 0.65. The fracture strain for the strain rate of $0.5 \times 10^9$ s$^{-1}$, $1 \times 10^8$ s$^{-1}$, $0.5 \times 10^8$ s$^{-1}$, $1.0 \times 10^7$ s$^{-1}$, and $0.5 \times 10^7$ s$^{-1}$ are found to be 0.3, 0.35, 0.43, 0.48, and 0.34 respectively. It can be seen that the nanowire structure at a strain rates of $0.5 \times 10^7$, $1 \times 10^8$, and $0.5 \times 10^9$ s$^{-1}$ show reorientation from [100]/{100} to the atomic thick chain without forming any pentagonal multi-shell nanobridge structure. This indicates instability in the nanowire without much plastic deformation and further loading causes complete fracture of the structure. However the structure at a strain rate of $1 \times 10^9$, $0.5 \times 10^8$ and $1 \times 10^7$ s$^{-1}$ show larger ranges of plastic strain and fracture strain as compared to the strain rate of $0.5 \times 10^7$, $1 \times 10^8$, and $0.5 \times 10^9$ s$^{-1}$ as shown in figure 4. It is also observed that for a given cross-sectional dimension and temperature, with various strain rate loadings, produce constant initial slope of the stress–strain curve as shown in figure 4, indicating a linear elastic and rate-insensitive response.

Furthermore, in order to investigate the role of various cross-sectional dimensions on the formation of the pentagonal multi-shell nanobridge structure, we considered six different cases of cross-sectional areas: $0.3615 \times 0.3615$, $0.723 \times 0.723$, $1.0845 \times 1.0845$, $1.446 \times 1.446$, $1.8075 \times 1.8075$ and $2.169 \times 2.169$ nm$^2$. Results show that only the nanowires with cross-sectional dimensions $<1.5$ nm reoriented from [100]/{100} to the stable {111} pentagonal multi-shell nanobridge structure, whereas the nanowires with $>1.5$ nm failed mainly by full or partial dislocation via twinning. Figure 5 shows a constant slope of the initial stress–strain curve for various cross-sectional dimensions at a strain rate of $1 \times 10^9$ s$^{-1}$, whereas a rate-insensitive elastic modulus was already observed in figure 4. Hence, the overall response is due to a rate and cross-section independent elastic modulus of $\sim$100 GPa before yielding. Figure 6(a) shows the yield stress and corresponding yield strain for varying cross-sectional areas. Decreasing yield stress and yield strain with increasing cross-sectional area can be seen. Similar results have been observed by Harold *et al* [48] for Cu nanowires with larger cross-sectional dimensions but without any new structure formation.

Furthermore, to find out the effect of initial residual stress on the true yield strain, the equilibrium yield strain has been calculated by extrapolating the initial slope of the stress–strain curves. The equilibrium yield strain is calculated as

$$\varepsilon^*_{\text{yield}} = \varepsilon_0 + \varepsilon_{\text{yield}} \tag{5}$$

where, $\varepsilon_{\text{yield}}$ is the yield strain of the current configuration, $\varepsilon^*_{\text{yield}}$ is the equilibrium yield strain (true yield strain), and $\varepsilon_0$ is the initial residual strain, which is calculated by drawing a tangent to the initial slope of the stress–strain curve. When the line intersect the $x$-axis (i.e. at zero stress level), it gives initial residual strain; that is the strain part which is due to the initial residual stresses. Figure 6(b) shows the yield stress and the corresponding equilibrium yield strain for varying cross-sectional area of the Cu nanowires. Our result shows that the value of $\varepsilon_0$ and $\varepsilon^*_{\text{yield}}$ decreases with increasing cross-sectional dimensions of the nanowires. This is due to fact that as the cross-sectional dimensions increase, the initial residual stress reduces. It is also found that for a given strain rate and temperature, the yield stress and the subsequent equilibrium yield strain decrease with increasing cross-sectional dimensions as shown in figure 6(b).

## 4. Conclusions

A stable pentagonal multi-shell nanobridge structure under high strain rate tensile loading on [100]/{100} square cross-sectional Cu nanowires has been found. Such a stable structure has enhanced mechanical strength properties such as higher fracture strain. From these results we anticipate applications of the pentagonal Cu nanowires with diameters of the order $\sim$1 nm in nano-electronic devices. In addition, the pentagonal multi-shell structures were found to have an inherent stability that is dependent on the external loading rate applied to the nanowires. The formation of a stable pentagonal multi-shell nanobridge structure has been observed for cross-sectional dimensions $<1.5$ nm whereas nanowires $>1.5$ nm show failure due to partial and full dislocation via twinning. Strain rate insensitive, and a cross-sectional dimension insensitive elastic modulus of $\sim$100 GPa is also found. Decreasing yield stress and yield strain have been observed with decreasing strain

rate for a given cross-sectional dimension of the nanowires. For a given strain rate with increasing cross-sectional area, decreasing yield stress and yield strain are also observed. The stability of the pentagonal multi-shell nanobridge structures can be characterized by a much larger plastic deformation and higher fracture strain. Further research work has to be carried out to find out the effect of surface stresses and the lateral surface orientation on the formation of pentagonal nanowires including defects.

## Acknowledgments

Vijay Kumar Sutrakar would like to thank R Raghunathan, Group Director, and C M Venkatesh, Head of the Mechanical Engineering Design Division, Aeronautical Development Establishment, Bangalore for their positive support and encouragement.

## References

[1] Wang B, Yin S, Wang G, Buldum B and Zhao J 2001 *Phys. Rev. Lett.* **86** 2046
[2] Bilalbegovic G 1998 *Phys. Rev.* B **58** 15412
[3] Tosatti E, Prestipino S, Kostlmeier S, Dal Corso A and Di Tolla F D 2001 *Science* **291** 288
[4] Bilalbegovic G 2000 *Solid State Commun.* **115** 73
[5] Torres J A, Tosatti E, Dal Corso A, Ercolessi F, Kohanoff J J, Di Tolla F D and Soler J M 1999 *Surf. Sci.* **426** L441
[6] Bilalbegovic G 2000 *Comput. Mater. Sci.* **18** 333
[7] Hwang H J and Kang J W 2002 *J. Korean Phys. Soc.* **40** 283
[8] Kang J W and Hwang H J 2002 *Mol. Simul.* **28** 1021
[9] Kang J W and Hwang H J 2002 *J. Phys.: Condens. Matter* **14** 2629–36
[10] Gulseren O, Erolessi F and Tosatti E 1998 *Phys. Rev. Lett.* **80** 3775
[11] Di Tolla F, Dal Corso A, Torres J A and Tosatti E 2000 *Surf. Sci.* **456** 947
[12] Gulseren O, Erolessi F and Tosatti E 1995 *Phys. Rev.* B **51** 7377
[13] Finbow G M, Lyden-Bell R M and McDonald I R 1997 *Mol. Phys.* **92** 705
[14] Wang B, Yin S, Wang G and Zhao J 2001 *J. Phys.: Condens. Matter* **13** L403
[15] Diao J and Gall K 2003 *Nat. Mater.* **2** 656–60
[16] Kondo Y and Takayanagi K 1997 *Phys. Rev. Lett.* **79** 18
[17] Diao J and Gall K 2004 *Phys. Rev.* B **70** 075413
[18] Lieber C M 2003 *MRS Bull.* **28** 7
[19] Patolsky F and Lieber C M 2005 *Mater. Today* **8** 4
[20] Huang M H and Mao S 2001 *Science* **292** 5523
[21] Dual X and Huang Y 2003 *Nature* **421** 241–5
[22] Arnold M S and Avouris P 2003 *J. Phys. Chem.* B **107** 659–63
[23] Wu Y and Xiang J 2004 *Nature* **430** 61–4
[24] Duan X and Hunag Y 2003 *Nature* **409** 66–9
[25] Terabe K and Hasegawa T 2005 *Nature* **433** 47–50
[26] Walter E C and Penner R M 2002 *Surf. Interface Anal.* **34** 409–12
[27] Comini E and Faglia G S 2002 *Appl. Phys. Lett.* **81** 10
[28] Cui Y and Wei Q 2001 *Science* **293** 5533
[29] Zhong Z and Wang D 2003 *Science* **302** 5649
[30] Lieberman D S and Wechsler M S 1955 *J. Appl. Phys.* **26** 4
[31] Stalder A and Durig U 1995 *Appl. Phys. Lett.* **68** 5
[32] Kondo Y and Takayanagi K 2000 *Science* **289** 5479
[33] Konishi Y and Motoyama M 2003 *J. Electroanal. Chem.* **559** 149–53
[34] Lisiecki I, Filankembo A, Sack-Kongehi H, Weiss K, Pileni M P and Urban J 2000 *Phys. Rev.* B **61** 4968
[35] Michaelian K, Rendon N and Garzon I L 1999 *Phys. Rev.* B **60** 2000
[36] Erkoc S 2000 *Physica* E **8** 210
[37] Li T X, Yin S Y, Ji Y L, Wang B L, Wang G H and Zhao J J 2000 *Phys. Lett.* A **267** 403
[38] Catlow C R A, Bulatov V L and Grimes R W 1997 *Nucl. Instrum. Methods Phys. Res.* B **122** 301
[39] Rongwu L, Zhengying P and Yukun H 1996 *Phys. Rev.* B **53** 4156
[40] Lammers U and Borstel G 1994 *Phys. Rev.* B **49** 17360
[41] Liang W, Tomer V and Zhou M 2003 *Nanowires and Nanobelts: Materials, Properties and Devices* ed Z L Wang (New York: Springer) pp 122–55
[42] Liang W and Zhou M 2004 *J. Mech. Eng. Sci.* **218** 6
[43] Liang W and Zhou M 2005 *J. Eng. Mater. Technol.* **127** 4
[44] Liang W and Zhou M 2006 *Phys. Rev.* B **73** 115409
[45] Liang W and Zhou M 2005 *Nano Lett.* **5** 10
[46] Park H S, Gall K and Zimmerman J A 2005 *Phys. Rev. Lett.* **95** 255504
[47] Ji C and Park H S 2006 *Appl. Phys. Lett.* **89** 181916
[48] Ji C and Park H S 2007 *Nanotechnology* **18** 305704
[49] Mehrez H and Ciraci S 1997 *Phys. Rev.* B **56** 12632
[50] Sen P, Gulseren O, Yildirim T, Batra I P and Ciraci S 2002 *Phys. Rev.* B **65** 235433
[51] Gonzalez J C, Rodrigues V, Bettini J, Rego L G C, Rocha A R, Coura P Z, Dantas S O, Sato F, Galvao D S and Ugarte D 2004 *Phys. Rev. Lett.* **93** 126103
[52] García-Mochales P, Paredes R, Peláez S and Serena P A 2008 *J. Nanomater.* **2008** 361464 doi:10.1155/2008/361464
[53] García-Mochales P, Paredes R, Peláez S and Serena P A 2008 *Nanotechnology* **19** 225704
[54] Daw M S and Baskes M I 1984 *Phys. Rev.* B **29** 6443–53
[55] Daw M S, Foiles S M and Baskes M I 1993 *Mater. Sci. Rep.* **9** 251–310
[56] Mishin Y, Mehl M, Papaconstantopoulos D A, Voter A F and Kress J D 2001 *Phys. Rev.* B **63** 224106
[57] Nose S 1984 *J. Chem. Phys.* **81** 511–9
[58] Hoover W G 1985 *Phys. Rev.* A **31** 1695–7
[59] Liang W and Zhou M 2003 *Nanotech* **2** www.nsti.org ISBN 0-9728422-1-7
[60] Rodrigues V and Bettini J 2002 *Phys. Rev.* B **65** 153402
[61] Liu Z and Bando Y 2003 *Adv. Mater.* **15** 303–5
[62] Liu Z and Yang Y 2003 *J. Phys. Chem.* B **107** 12658–61
[63] Wang Y and Yang J 2004 *Nanotechnology* **15** 1437–40
[64] Swope W C, Anderson H C, Berens P H and Wilson K R 1982 *J. Chem. Phys.* **76** 637–49
[65] Plimpton S J 1995 *J. Comput. Phys.* **117** 1–19
[66] LAMMPS 2007 http://www.cs.sandia.gov/∼sjplimp/lammps.html
[67] Zhou M 2003 *Proc. R. Soc.* A **459** 2347–92
[68] Sanchez-Portal D, Artacho E, Junquera J, Ordejon P, Garica A and Soler J M 1999 *Phys. Rev. Lett.* **83** 3884–7